APPLICATION OF ELECTRON DIFFRACTION TO BIOLOGICAL ELECTRON MICROSCOPY

ROBERT M. GLAESER *and* GARETH THOMAS

From the Division of Medical Physics and Donner Laboratory, and the Department of Materials Science and Engineering and Inorganic Materials Research Division, University of California, Berkeley, California 94720

ABSTRACT Three methods by which electron diffraction may be applied to problems in electron microscopy are discussed from a fundamental point of view, and experimental applications with biological specimens are demonstrated for each case. It is shown that wide-angle electron diffraction provides valuable information for evaluating specimen damage that can occur either during specimen preparation or while in the electron beam. Dark-field electron microscopy can be used both to enhance the image contrast and to provide highly restricted and therefore highly specific information about the object. Low-angle electron diffraction provides quantitative information about the object structure in the range from 20 A to $\sim$ 1000 A. Low-angle electron diffraction also demonstrates the important role of Fourier contrast with biological specimens, which are usually characterized by structural features with dimensions of 20 A or larger.

INTRODUCTION

There are at least three major ways in which the application of electron diffraction can contribute to biological electron microscopy. One important way is through the application of wide-angle, selected-area diffraction in evaluating damage inflicted upon the specimen. For example, this might be damage produced through exposure to the electron beam, or it might be damage produced in the preparation of the specimen. A second useful application is the use of selected-area diffraction in connection with dark-field electron microscopy. This technique can be used to obtain highly specific information about the object, and it can also be used for enhanced image contrast. The third, and perhaps most important application of electron diffraction, comes in appreciating the very important role of Fourier Contrast in image formation with biological specimens. By Fourier Contrast we mean the general type of image contrast that results when coherently (elastically) scattered electrons are recombined by a lens. According to the diffraction theory or Abbe theory, the in-focus image thus produced is the Fourier synthesis of the complex scattering amplitude. (Abbe, 1873; Porter, 1906; Uyeda, 1955, 1956; Cowley and Moodie, 1957 *a*, *b*, *c*; Heidenreich, 1964, especially chapters V and X)

For each of these applications the experimental techniques and the theoretical foundations are well known in electron microscopy applied to the physical sciences, particularly in materials research. However, the several techniques have seldom been used with biological specimens; nevertheless a review covering applications of electron diffraction in biological electron microscopy has already been given (Parsons, 1968). The interpretation of image contrast and diffraction effects requires a knowledge of the fundamentals of diffraction theory. The geometrical concepts of reciprocal lattice and reflecting sphere are especially useful for selected area diffraction and dark field imaging techniques (see for example Thomas, 1962; Hirsch et al., 1965).

ELECTRON DIFFRACTION TECHNIQUES

Selected Area, Wide-Angle Diffraction

The basic technique of selected area diffraction is described in most books devoted to electron microscopy (see as examples Hirsch et al., 1965; Hall, 1966). The Fraunhofer diffraction pattern itself is formed in the back focal plane of the objective lens, in accordance with the normal principles of optics. When the lens current for the intermediate lens is decreased its focal length increases until the back focal plane of the objective lens, together with the diffraction pattern, is imaged by the intermediate lens. The final projector lens in turn magnifies the diffraction pattern. The effective camera length for this method of diffraction is usually a few hundred millimeters, so that the technique is useful for Bragg reflections ranging from tenths of Angstroms up to 20 A or somewhat more.

The method of selected area diffraction possesses several advantages. First of all the technique permits the specimen to be examined in the same position as is normally used for direct microscopy. This gives one the ability to examine the same specimen alternately in real space (as in the focused image) and in reciprocal space (as the Fraunhofer diffraction pattern), simply by changing the lens current of the intermediate lens. A second advantage is that one may observe diffraction patterns from extremely small crystals. Lens aberrations limit the smallest useful field-of-view to about 1 μ diameter at 100 kv, but to only 0.05 μ diameter at 1 Mev. Another advantage of this method is that the diffraction pattern normally is directly visible on the fluorescent screen. Depending upon the intensity of illumination, the diffraction pattern can be recorded on photographic plates with exposure times ranging from a fraction of a second to a few hundred seconds.

Many biological specimens are extremely sensitive to damage in the electron beam, and as a result it is not possible to observe a diffraction pattern using the same technique that is satisfactory for inorganic crystals. Each of the following suggestions have been found to contribute to the preservation of beam-sensitive crystals: decrease the beam current to a minimum; operate the first condenser lens at maximum excitation (maximum lens current); use a very small condenser aper-

ture—certainly no larger than 100 μ in diameter; operate the second condenser lens at nearly maximum excitation (i.e., with as short a focal length as possible). Not only is the current density on the specimen minimized by using a short focal length for C2, but also the beam divergence is minimized (Hall, 1966 page 153). The additional benefit of "parallel" illumination assures optimal coherence and optimal angular resolution in the diffraction pattern.

Low-Angle Diffraction Techniques

In the work reported here we have used the three-lens technique first described by Ferrier and Murray (Ferrier and Murray, 1966; see also the closely related technique of Bassett and Keller, 1964). With nonconducting biological specimens it is *essential* to coat the specimens lightly with carbon, or in some other way to prevent the charging up which can deflect and distort the electron beam as well as damage the specimen. The specimen is left in the position normally used for high resolution microscopy, but both the objective and the intermediate lenses are turned off. The first condenser lens is usually operated at maximum excitation, and the lens current in the second condenser lens is decreased until a minimum spot size is observed on the fluorescent screen. This optical system provides a slightly convergent illumination at the specimen, so that the transmitted and the scattered electrons are all brought to focus on the object plane of the final projector lens. The effective camera length is controlled by varying the magnification of the projector lens. The effective camera length is usually on the order of ten to one hundred meters, and it is relatively easy to achieve an angular resolution corresponding to Bragg reflections from periodic spacings of 500-1000 A. Diffraction patterns from ordered structures approximately 5-10 μ in diameter and larger can usually be seen directly on the fluorescent screen, and the exposure times required for photographic recording range again from a fraction of a second to a few hundred seconds.

Low-angle electron diffraction suffers a disadvantage due to the large fraction of inelastic electrons scattered in the forward direction. These form a diffuse background at small angles, and thereby decrease the contrast in the diffraction pattern. Consequently it is necessary to maximize the signal-to-background ratio. This is achieved by limiting the area illuminated as closely as possible to just that area from which diffraction data are sought. In this regard we have found it useful to employ very small apertures in the condenser lens. The data reported here were obtained with 10 or 15 μ diameter apertures purchased from C. W. French, Inc. (Weston, Mass.). The objective aperture can also be used as a field-limiting aperture (Ferrier and Murray, 1966), and we have found this to be useful if the condenser aperture happened to possess peripheral or satellite openings.

The possibilities for low-angle selected area diffraction by the three lens method are partially limited by difficulties of optical alignment. The positioning of the condenser aperture is the most critical adjustment, and if it is not properly centered one

may expect to see the projected image of the aperture "sweep" over a portion of the specimen as the lens current in the second condenser is varied. Once the aperture has been centered the condenser lens current can be increased and the specimen can be moved until a desired area is centered in the limited field-of-view which is thereby projected on the screen. Since under these circumstances the magnification is quite low, one is limited to identifying areas, at low resolution, with dimensions on the order of 5 μ or larger.

If an area of the specimen is found which gives rise to a diffraction pattern, it is possible with some difficulty to examine the same area by high resolution microscopy. In order to do so, one must gradually activate the intermediate and the objective lenses, continually adjusting the specimen position so as to compensate for the various image rotations (and translations) that occur. It is recommended to first activate the objective lens fully (preferably at a low excitation of the final projector lens) and then to adjust the intermediate and projector lenses. With the specimen in position it is then usually necessary to make some final alignments, particularly of the condenser and objective apertures.

EVALUATION OF SPECIMEN DAMAGE

Specimen Damage in the Electron Beam

Wide-angle, selected-area electron diffraction is a powerful technique for the evaluation of damage produced in crystalline materials by exposure to the electron beam. The existence of sharp maxima in the diffraction pattern imply the existence of well defined periodicities in the structure of the object. If the structure is damaged in some way, the periodicity is necessarily degraded in some way. One may then expect to observe the diffraction maxima being broadened, streaked, or converted into rings depending upon the types of damage that are possible.[1] The structural level at which the damage occurs can be deduced by observing which diffraction maxima are being affected, since structural periodicities of varying size are related to the scattering angle through Bragg's Law:

$$d_{hkl} = \frac{\lambda}{2 \sin \theta}$$

where d_{hkl} is the spatial separation between repeating structures, λ is the electron wavelength, and 2θ is the scattering angle.

It is evident that electron microscope specimens can be damaged by a variety of mechanisms. Specimen heating is one mechanism that is well known to most microscope users. Other mechanisms include the interaction of ionized gases with the specimen, and ultimately, direct radiation damage to the specimen by the electron

[1] The reverse process is also possible in some circumstances; initially amorphous specimens can be crystallized in the electron beam and broad maxima can correspondingly become sharpened.

beam. Direct radiation damage poses a fundamental limit to the preservation of specimens, but certain improvements in instrumentation might be expected to decrease the amount of damage introduced by other mechanisms. Some of the improvements now under development in many laboratories include high vacuum microscopes to decrease the concentration of ionized gases, high voltage microscopes to decrease ionization (due to the lowering of scattering cross-sections) and heating within the specimen, image intensifiers to allow lower levels of illumination (and thus decreased rates or ionization and heating), wet-specimen stages with controlled partial humidity to avoid dehydration, and low temperature specimen stages to decrease heating and to immobilize structures even if they become damaged. We suggest here that selected area diffraction can be a powerful tool for evaluating the usefulness of such devices in the preservation of biological specimens.

In the evaluation of damage produced in the specimen, selected area diffraction is superior to direct microscopy in two important ways. First of all it is well known that high-resolution image-information is perturbed by the various lens aberrations, mechanical instabilities, and electrical instabilities. This is also true for high-resolution diffraction-information. However, it is much easier for high-resolution information in the image mode to become obscured by these aberrations and instabilities than is the case for the diffraction mode. In the diffraction mode it is therefore perfectly easy to observe the preservation of structure down to 1 A or less. The second point is that a diffraction pattern may be observed at much lower levels of illumination than that which is required for focusing an image at 10,000 magnification or greater. The level of illumination required to focus and record an image at moderate to high magnification can be so great that damage to the specimen is completed in a period much shorter than the integration time of the eye or the exposure time for the photographic plate. In the diffraction mode the level of illumination can be decreased to the point that changes in the specimen occur over a time period which can readily be observed visually or recorded photographically. In effect one is able to attain both a better spatial resolution and a better time resolution when using electron diffraction to evaluate beam-induced damage in the specimen.

We have begun to apply the selected area diffraction technique to crystalline amino acids, in order to investigate the type of beam sensitivity that might be encountered with more complex structures such as proteins, viruses, cell membranes, etc. Electron diffraction patterns were attempted with several amino acids (alanine, cysteine, cystine, glutamic acid, glycine, phenylalanine, and valine), and in most cases some patterns could be recorded. The greatest success was obtained with l-valine, as this amino acid produced specimens more conveniently than did the others and was as resistant to beam damage as any of the other amino acids.

Specimens of crystalline l-valine can be prepared by solvent evaporation from distilled water on formvar coated grids. A large percentage of the flat, dendritic crystals formed in this way are thin enough to be suitable for diffraction and micro-

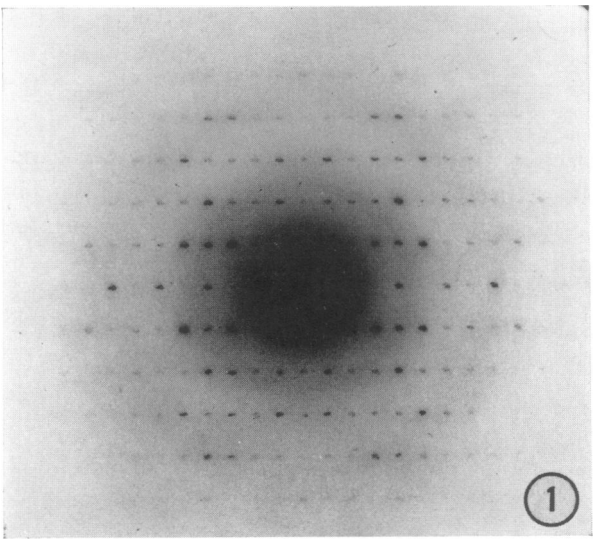

FIGURE 1 Wide-angle selected area electron diffraction pattern obtained from a mosaic single crystal of l-valine. Sharp diffraction maxima are observed out to crystal spacings of 1.06 A.

scopy. Fig. 1 is one example of the symmetrical diffraction patterns which could be recorded photographically with illumination levels corresponding to photographic exposure times between 20 sec and 200 sec. Similar patterns have been obtained in our laboratories by several persons, and the Bragg spacings have been carefully indexed on three occasions using the ring-pattern from evaporated gold to calibrate the camera constant. If the pattern in Fig. 1 is assumed to be the (*hkO*) reciprocal lattice plane, then the deduced unit cell dimensions $a = 9.70$ (± 0.05) A, $b = 5.31$ (± 0.05) A are consistent, within experimental error, with the monoclinic unit cell of l-valine measured previously by X-ray diffraction (Tsuboi, Takenishi, and Iitaka, 1959).

All specimens were extremely sensitive to degradation in the electron beam, and the most delicate technique was required in order to observe the wide-angle diffraction pattern. In order to find suitable diffraction patterns it is necessary to scan the specimen grid in the selected area diffraction mode rather than in the direct-image mode, since the relatively large amount of specimen illumination required to see an image leads to an extremely rapid fading of the entire diffraction pattern. A serious implication of this observation is that the high-resolution structure in any unfixed, nonembedded biomolecular material may similarly become disordered by the amounts of electron-beam illumination that are typically used in high-magnification electron microscopy. In any event these observations suggest one possible explanation as to why electron micrographs of negatively stained viruses, proteins and simi-

lar materials show virtually no interpretable detail below a resolution of approximately 15-20 A.

Specimen Damage in Preparation

In contemplating electron diffraction and high resolution electron microscopy of complex biological structures one must evaluate the damage and disordering involved in specimen preparation as well as that associated with too great an exposure to the electron beam. A reasonable objective in this regard would be to prepare a specimen of crystalline protein or virus which was capable of producing a wide-angle diffraction pattern. This has not yet been achieved, and it is therefore worth discussing what some of the causes may be for the lack of success to date. It has been suggested that biological structures may not tolerate the removal of water, or at least not the tightly bound ("hydrogen bonded") water (Parsons, 1966; Murray and Ferrier, 1968). This would indeed seem an important consideration on the basis of what is now known of the role of water in protein and other macromolecular structures, especially the phenomenon of hydrophobic bonding. Independently of the theoretical dependence of protein structure upon bound and free water one would also expect that the surface tension effects encountered in air-drying of specimens would result in serious flattening and distortion of the structure (Anderson, 1956). This may also be a contributing factor to the limit of resolution obtainable with negatively stained materials.

It may be postulated that chemical fixation (molecular cross-linking) and embedding procedures would better preserve biomolecular structure in the face of the removal of water. Recent observations of the circular dichroism of proteins in solution and of cell membrane proteins have shown that the commonly used fixatives can in fact alter the conformation of proteins; the smallest effect was observed with gluteraldehyde, but even there it was estimated that 20-30% of the helical content of the protein was disrupted (Lenard and Singer, 1968). On the other hand, it has been demonstrated that at least some crystalline proteins can be completely cross-linked by gluteraldehyde with a minimal effect upon their X-ray diffraction patterns (Hass, 1968). Optical studies have also been made of the effect upon protein structure of non-aqueous solvents similar to those used in dehydration and embedment of biological specimens (Singer, 1962; Sage and Singer, 1962; Tanford et al., 1962). Here again a severe alteration of the native protein has been observed.

Our own studies in this regard have been devoted extensively to crystalline lactoglobulin and to crystalline ferritin, but we have also investigated crystalline ribonuclease, lysozyme, and myoglobin. Crystalline structure of unfixed proteins could usually be well preserved at the microscopical level by passage into propylene glycol or into aquon (a description of aquon embedment is given by Glauert, 1965), but this is not, in general, true for passage into ethanol. Crystalline proteins that could be passed into 100% propylene glycol were completely dissolved, however, when

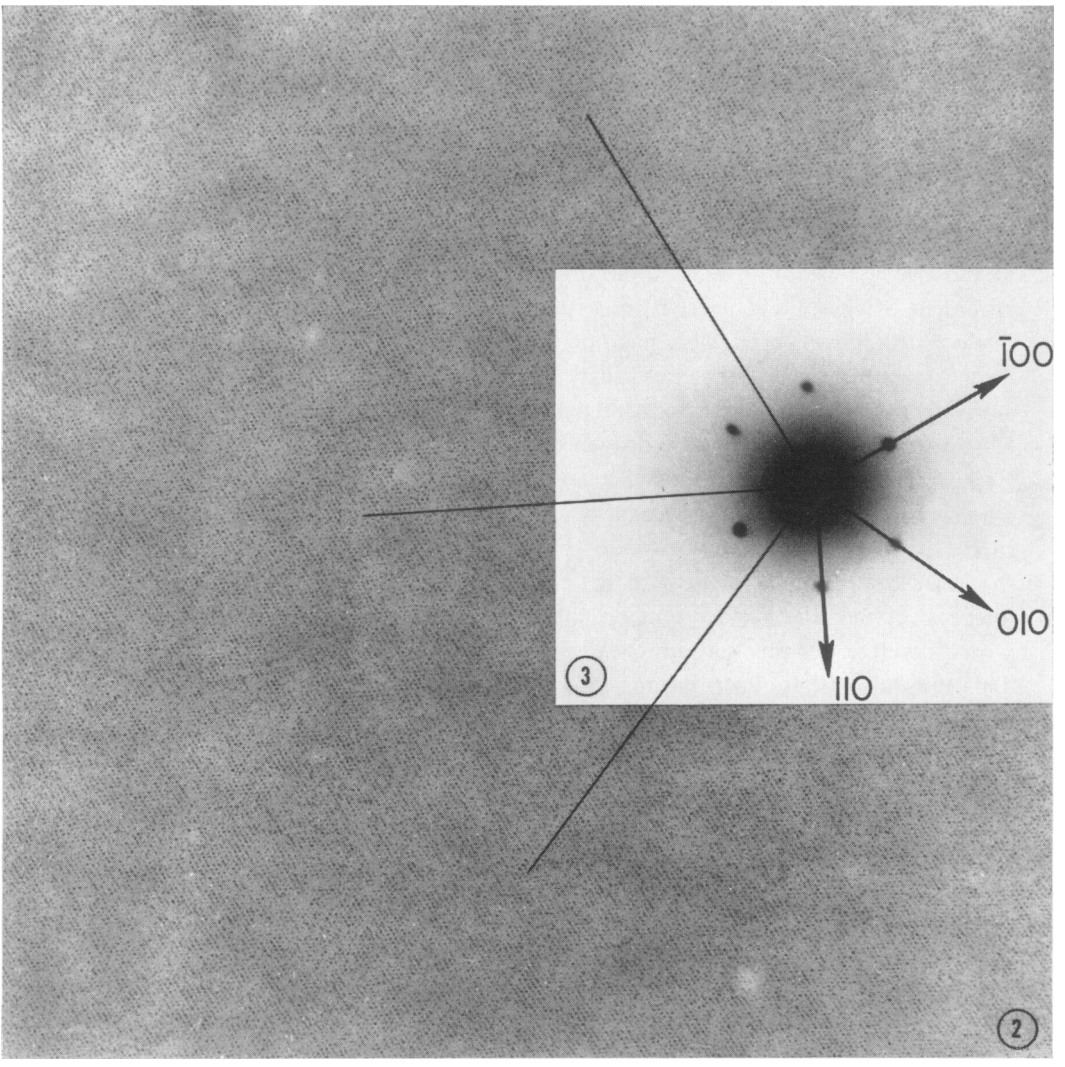

FIGURE 2 Unstained thin section of crystalline ferritin. There is a wide variation in the amount of iron hydroxide bound to each protein molecule, and the amount of iron bound does not influence the ability of the molecule to be incorporated into the crystal.

FIGURE 3 Low-angle electron diffraction pattern obtained with the same unstained thin section of crystalline ferritin as shown in Fig. 2. Note that both the crystal lattice and diffraction pattern show a distorted twofold symmetry. The distortion may be due to compression effects in sectioning, or it may be due to the plane of sectioning being poorly aligned with a simple crystal-axis. The presumed axes are indicated on the figure.

passed into the usual epon embedment. Crystalline lactoglobulin retained its microscopic structure and birefringence when embedded in aquon, but this material has not yet been successfully sectioned. These and other methods are still under development.

Our most successful preparation technique to date has been one very similar to that developed recently by Pease (Pease, 1966; Pease, 1967). Fig. 2 is an example of a micrograph of an unstained thin section of crystalline ferritin. Purified ferritin was purchased from Nutritional Biochemicals Corporation (Cleveland, Ohio) and recrystallized by addition of 10% $CdSO_4$ according to the method of Granick (1942). The crystalline protein was then passed into 70% propylene glycol, 30% mother liquor. The crystals were next transferred to a solution of 70% propylene glycol, 2.5% gluteraldehyde, and 27.5% distilled water. Following fixation for 2 hr the crystals were transferred through mixtures of propylene glycol and epon, and finally embedded in the 1:1 epon A, epon B mixture of Luft (Luft, 1961). Fig. 3 is a low angle electron diffraction pattern obtained from an area of a specimen which included the area reproduced in Fig. 2. The relative sharpness of the Bragg maxima observed here indicates that the position of each molecule in the unit cell has been preserved exceedingly well by the technique. The absence of higher order reflections would seem to be a result of the considerable degree of density disorder between the individual molecular positions. The variation in molecular density almost certainly is not an artifact of preparation, since it is well known that native ferritin is characterized by a wide distribution in the amount of iron hydroxide bound to each protein molecule (Farrant and Hodge, 1956; Fischback and Anderegg, 1965). The results that have been obtained so far clearly show that low-angle as well as wide-angle selected-area diffraction can be an invaluable diagnostic technique for evaluating and improving upon the presently available specimen-preparation methods.

DARK-FIELD ELECTRON MICROSCOPY

A high resolution dark-field image is obtained by allowing one diffracted beam to pass along the optic axis. Such an arrangement is obtained by either mechanically tilting the electron gun by means of the gun translators (Maher et al., 1965) or by electrical deflection of the beam as is now possible on most modern microscopes. The advantage of this method is that the specimen itself is not moved or tilted, and abberations due to inelastic scattering are progressively reduced as the diffraction angle is increased. Astigmatism limits the useful angle to about 3° at 100 kv or $1\frac{1}{2}$° at 500 kv. It is important to realize that the dark-field image must be obtained from the negative diffraction vector to that which operates in normal bright field, as is illustrated in Fig. 4. Thus one tilts in the opposite direction to that which one might expect. Simply tilt the transmitted beam over towards the position of the (*hkl*) beam that was operating in bright field until ($\bar{h}\bar{k}\bar{l}$) is on the optic axis. This beam will have maximum intensity. If one tilts the *hkl* beam to the center, intensity is lost

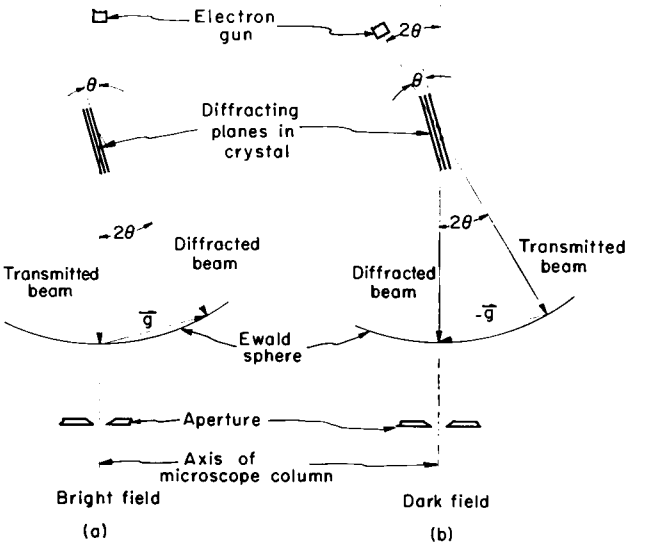

FIGURE 4 Imaging conditions for (*a*) normal bright field and (*b*) high resolution dark-field microscopy. Notice that for maximum dark-field intensity the gun tilt or beam deflection must be done in the opposite sense to that for bright field.

because this spot moves off the reflecting sphere (Fig. 4 *b*). This effect is important for all reflections occurring at angles of $\frac{1}{2}°$ or larger.

A simple method of dark field imaging is to translate the objective aperture over to the diffraction spot of interest. In this case however the image quality is poor because of chromatic and spherical aberration. Nevertheless the aperture method is quick and useful for exploratory work until the high resolution image is required. In addition to these precedures it is also necessary to use a double-tilt (or tilt-rotation) specimen stage so as to tilt various reflections into operation. In complex materials the combination of imaging the diffraction pattern by dark field techniques enables the patterns to be more easily solved as well as providing information on contrast mechanisms.

The preselection of data in Fourier space (reciprocal space) which necessarily occurs in dark-field microscopy provides images containing highly restricted and specific information relative to the normal bright-field images. The specifically restricted nature of the image information can be of considerable value, but the specificity is often gained at the loss of a general visual comprehension concerning the structure of the object. The difference in visual comprehension can be experienced by comparing the two images in Figs. 5 and 6. The specimen in this case is a chromium-shadowed carbon replica of a human red blood cell, prepared by the freeze-drying technique (Glaeser, et al., 1966). Crystallization of the vacuum-evaporated metal produces separate grains approximately 30 A on edge. Fig. 5 shows, as bright spots, just those crystallites for which the (111) Bragg reflected

FIGURE 5 Dark-field electron micrograph of a chromium-shadowed human red blood cell. This image was produced by moving the objective aperture off-axis until it transmitted a portion of the (111) Debye-Scherrer ring. Individual microcrystals which are oriented so that they satisfy the appropriate Bragg condition are thereby imaged as bright spots. Note that the crystal size formed over the cell surface is the same as that formed over the (mica) substrate.

electrons pass through the off-axis objective aperture. Fig. 5 further demonstrates that the crystal grain-size over the organic surfaces of the RBC is the same as that over the substrate (in this case, freshly cleaved mica). On the other hand, Fig. 6 clearly conveys the impression that the morphology of the red blood cell is that of a biconcave disk. In addition the red blood cell in this type of preparation has a

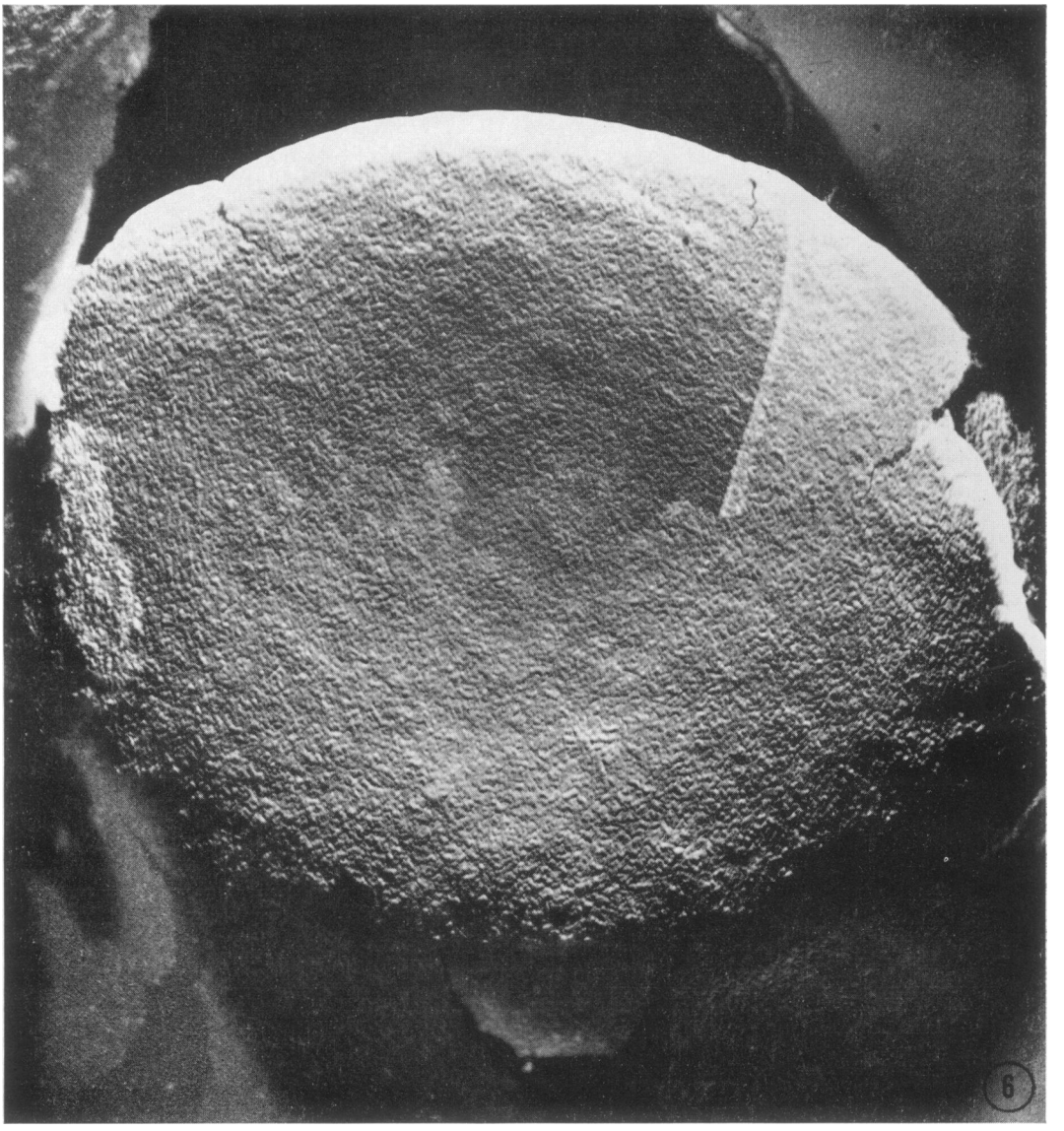

FIGURE 6 Bright-field electron micrograph of the same chromium-shadowed human red blood cell as shown in Fig. 4. In this case the electrons scattered at wide angles by the chromium are all stopped by the objective aperture.

pebbly or cobble-stone surface-structure which is not at all appreciated in the dark-field image.

A further example of the difference in visual comprehension is provided by a comparison of the dark-field and the bright-field images of crystalline l-valine. Fig. 7 is a dark-field micrograph revealing extinction contours in bright contrast. The

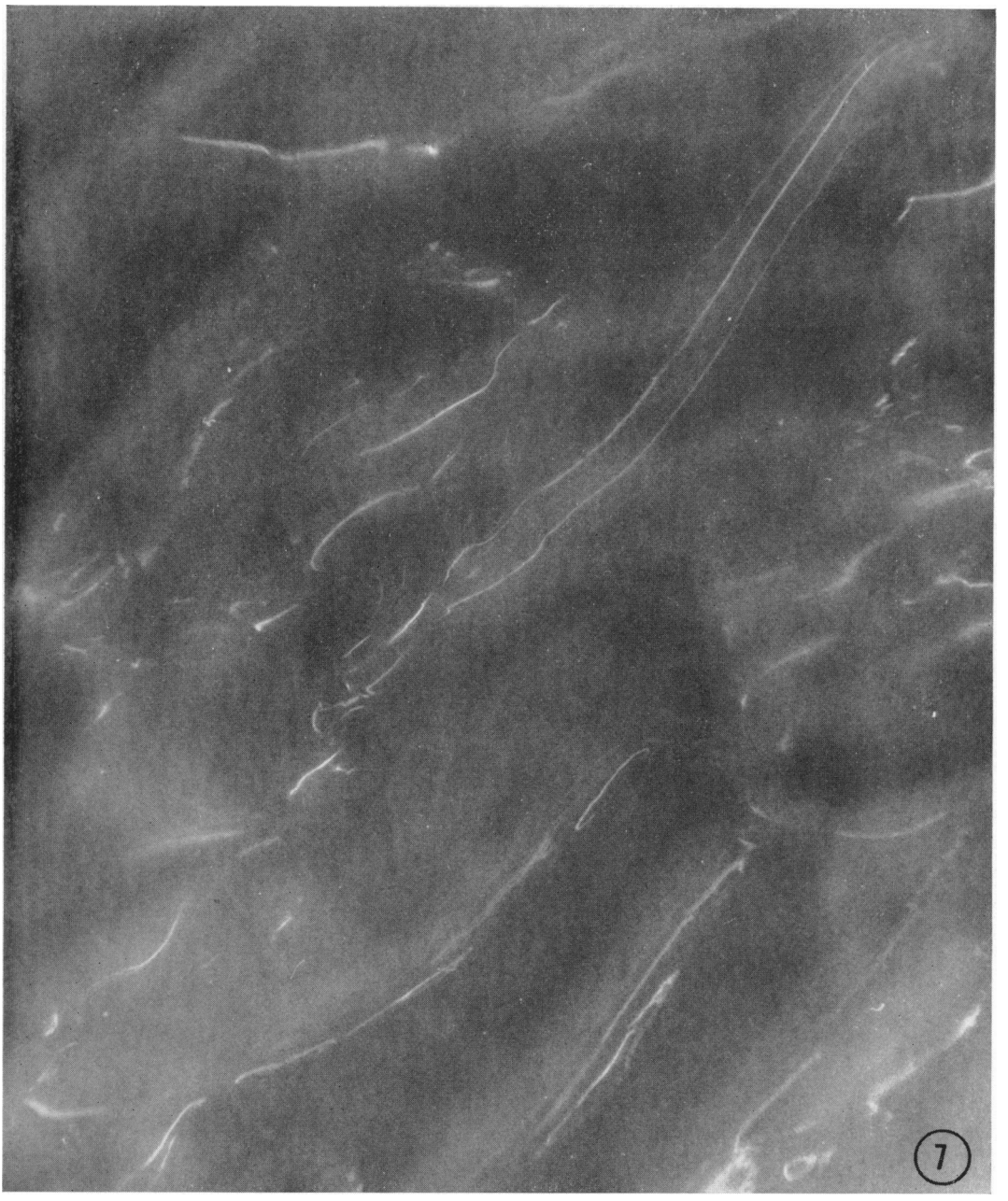

FIGURE 7 Dark-field electron micrograph of crystalline l-valine. This micrograph demonstrates through the localized regions of bright contrast that only a small portion of the single crystals satisfies the Bragg condition for a given reflection. This may be due to a slight warping of the crystal or some other form of mosaic structure.

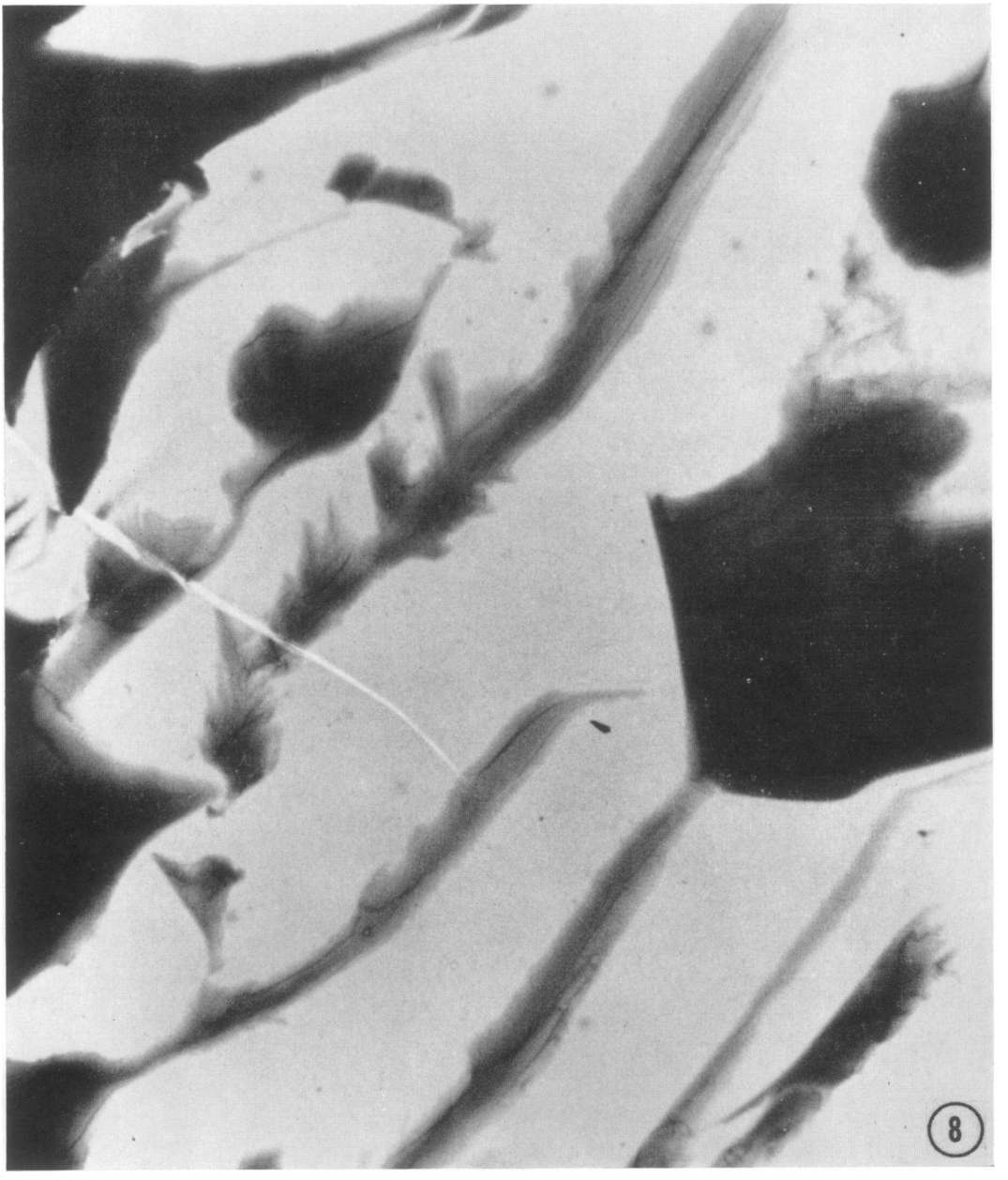

FIGURE 8 Bright-field electron micrograph of the same field of crystalline l-valine as is shown in Fig. 6. This micrograph shows clearly the dendritic morphology of the several crystals present in the field.

portions of the crystal appearing bright in the dark-field image are uniquely associated with one of the Bragg maxima that are observed in the diffraction pattern (cf. Fig. 1). The image shows in an unambiguous way that only a portion of the crystal participates in diffraction for a given Bragg maximum, and thereby confirms the mosaic nature of these single crystals. It is not at all evident, however, what the morphology of the crystal is; for example, whether the entire field-of-view is a single crystal or a number of crystals. These more general points of information are better conveyed in the bright-field image shown in Fig. 8. The micrographs in Fig. 7 and in Fig. 8 were obtained with the aid of an AEI image intensifier at an electron optical magnification of 2,500 (Glaeser et al., 1968). The field of view shown here produced a single crystal pattern similar to that in Fig. 1. No noticeable change in the pattern was seen in diffraction patterns recorded separately before and after the micrographs were recorded.

Another feature evident in dark-field micrographs is the relatively high contrast that results from exclusion of the forward-scattered beam. This kind of enhanced contrast is fundamentally different in nature from that which can be accomplished through background subtraction. It furthermore has the advantage that the enhanced contrast is available at the time of imaging and focusing. It may be expected that dark-field microscopy will be of considerable value in high voltage electron microscopy with biological specimens. In this case low image contrast may be a problem because most of the electron energy remains in the transmitted beam. Exclusion of this beam is necessary to obtain better contrast. Dark-field images formed by low-angle scattered electrons would be particularly useful with biological specimens, since biological structures have relatively large characteristic dimensions. Low-angle dark-field images have been reported with polystyrene latex spheres (Yeh and Geil, 1967). These images are actually extremely difficult to obtain, since the objective aperture must be positioned with great accuracy: the edge of the objective aperture must be positioned between the central beam and the first Bragg maximum at the radial distance $R = \lambda f/d = 2\theta f$ where λ = the electron wavelength, f = the objective lens focal length, and d = the spacing of reflecting planes for the Bragg angle, θ.

LOW-ANGLE FOURIER CONTRAST

Electron Diffraction and Fourier Transforms

Image formation in any type of optical system that has a coherent plane-wave source is intimately related to coherent scattering, i.e. diffraction by the object, regardless of whether the object has a crystalline substructure or not. Both the mathematical description of coherent scattering and the mathematical description of the subsequent image construction rely greatly upon the complex harmonic function representation of the Fourier transform. It is appropriate therefore to designate as *Fourier Contrast* the variations in image intensity that result from coherent scat-

tering of electron-waves in the object and their subsequent recombination by the objective lens. As is shown later in this section, the spatial coherence obtainable in the electron beam of a conventional electron microscope[2] is great enough to provide sharp diffraction maxima from specimens with periodicities exceeding 500 A. Indeed, Curtis et al. have been able to resolve electron diffraction maxima corresponding to spatial periodicities of more than 10^5 A (Curtis et al., 1967).

It is well known in optics that a Fraunhofer diffraction pattern is produced in the back focal plane of a lens when the object is illuminated by coherent plane-waves. Furthermore, it is a familiar theorem of scattering theory that the complex scattering amplitude in the Fraunhofer diffraction pattern is proportional to the Fourier transform of the scattering potential in the object. This theorem assumes, however, that multiple scattering events (i.e. dynamical scattering) can be neglected. The diffraction pattern is not, however, the complete Fourier transform of the scattering potential. The diffraction pattern is actually the intersection of the Ewald sphere with the complete, three-dimensional Fourier transform.

For those situations where the plane-wave scattering amplitude can be described as the Fourier transform of the structure in the object, one may subsequently apply Fourier transform theory in the description of the image. Before considering the image, however, it may be worthwhile to review some essential properties of the Fourier transform as it is related to scattering theory. To begin with, the structure of an object can generally be described as some function in three dimensional space. The electrostatic (coulomb) potential due to both the nuclei and the electrons is the spatial function of particular importance in electron scattering processes. A mathematically equivalent description of the structure of an object can be given as the Fourier transform of the structure that exists in real space (more properly, of the mathematical function describing that structure). The Fourier transform itself is described in a frequency space for which the coordinates are reciprocal to those of the real-space coordinates. The two representations are completely equivalent so one can transform back and forth from real space to reciprocal space, and from reciprocal space to real space through the Fourier transform.

The diffraction theory or the Abbe theory of microscopic vision considers first of all that a Fraunhofer diffraction pattern is produced in the objective lens back focal plane. This diffraction pattern is a small portion of the (complete) reciprocal-space representation of the object. At the objective lens image plane the various components of the complex scattering amplitude (diffraction pattern) are again combined to give an image. For a perfect lens, the *wave-amplitude* in the image is a Fourier synthesis of the reciprocal space representation found at the back focal plane. This Fourier image represents the combination of all reflections accepted by the objective lens. The typical high resolution "direct lattice" image is usually due to two beams 000, *hkl*, and therefore consists of alternating light and dark lines.

[2] An Hitachi HU 11 and an Hitachi HU 125 were used for most of the work reported here.

But for large-spacing crystals, complex images (cf. Fig. 2) can be obtained because many beams (cf. Fig. 3) are involved in the interference pattern (i.e., many beams are associated with the 000 beam in the small angle region). For adequate contrast the *hkl* beams must have adequate intensity, and specimen staining is often necessary to achieve this. It is important to note that it is the amplitude of the wave function at the image plane, and not the intensity, which is related by the Fourier transform to the complex scattering amplitude generated by the original object. Because of the important role played by the Fourier transform in this description of image formation it would seem appropriate to describe the resulting image contrast as "Fourier contrast". A more detailed description of out-of-focus as well as in-focus Fourier contrast images can be found in the papers of Cowley and Moodie (Cowley and Moodie, 1957 *a*, *b*, *c*). We emphasize again that the validity of this theory requires that coherent, plane-wave illumination be employed, that dynamical (multiple scattering) effects are negligible, and that non-coherent (inelastic) scattering events are either negligible or that the inelastically scattered electrons may be filtered from the image. Additional modifications to the theory must necessarily be added to account for the optical transfer function of any real system (for a discussion of optical transfer function theory see Goodman, 1968). Examples of such transfer functions would be a quarter wave plate in the objective lens back focal plane, as in the Zernike phase contrast microscope, or the spatial-frequency dependent phase shifts that are introduced by spherical aberration and other instrumental defects.

The Fourier Projection Theorem

There is a theorem, commonly used in crystallographic work (e.g. Vainshtein, 1964 chapter 4), that the Fourier synthesis from a two dimensional plane in reciprocal space is proportional to the two dimensional projection of the scattering potential:

$$V(x,y) \equiv \int V(x,y,z)\, dz \propto \iint \Phi(S_x, S_y, 0)\, e^{i2\pi(S_x \cdot X + S_y \cdot Y)}\, dS_x\, dS_y$$

where

$V(x, y, z)$ = the scattering potential,

$\Phi(S_x, S_y, S_z)$ = the complex scattering amplitude,

S_x, S_y, S_z = cartesian components of vectors in reciprocal space.

In the case of kinematical scattering, $V(\bar{r})$ is a real function and does not change sign. Thus the square root of the image intensities in a Fourier contrast image could be interpreted as being proportional to the z-projection of the structure of the object. The concept that the electron microscope image is the z-projection of the mass-thickness of the object has been employed recently by DeRosier and Klug as the

basis for numerical analysis of electron micrographs. With the appropriate numerical analysis it is possible to remove image-noise associated with the specimen substrate, and it is even possible to make a three-dimensional construction from single micrographs of objects that possess cylindrical or helical symmetry (DeRosier and Klug, 1968).

The actual Fourier contrast image differs from the true Fourier projection in that the former is produced by a Fourier synthesis from the Ewald sphere, which is not a true plane in reciprocal space. It would seem that the curvature of the Ewald sphere at high resolution as well as the effects of the optical transfer function introduce problems that still require investigation and elucidation (Glaeser and Thomas, 1968). It would seem likely, however, that the low-resolution imaging of sufficiently large structures by Fourier contrast does correspond closely to the projection of the scattering potential onto a plane; in this case the scattering occurs at very small angles, and over this restricted angular range the Ewald sphere closely approximates a plane.

Effect of the Objective Aperture upon Fourier Contrast Images

The objective aperture is located effectively in the objective lens back focal plane. Consequently the aperture serves to intercept that portion of the diffraction pattern which falls on the opaque area of the aperture, and only that portion of the diffraction pattern that falls within the open area of the aperture can contribute to the subsequent Fourier synthesis of the image. The mathematical effect of the aperture is properly described as a truncation of the Fourier synthesis. It is evident that if the Fourier synthesis is truncated beyond some spatial frequency, then there can be no information in the image concerning the structure beyond the corresponding spatial resolution. Consequently, the greater the desired degree of resolution, the larger must be the objective aperture in order to pass the higher-frequency components of the Fourier spectrum. In the usual arrangement the objective aperture is a circular opening, centered on the optical axis. In such a case the aperture symmetrically admits all Fourier components up to a limiting spatial frequency. It is readily estimated from the Bragg equation that under normal circumstances the objective aperture permits the Fourier resolution of all structures with characteristic dimensions of at least 10 A and larger. With a large objective aperture and a very short focal length it is even possible to resolve lattice spacings of less than 2 A in metals (Komoda, 1966). Some examples of how the objective aperture affects the resolution are presented in Table I, but these must be calculated independently for each instrumental value of focal length, aperture diameter, and electron wavelength.

The objective aperture will remarkably influence contrast, as well as resolution, in Fourier images. However, the way by which contrast is altered differs fundamentally from the usual description in which the aperture has an effect equivalent to the highly localized absorption of electrons in the specimen. In the latter picture

TABLE I

LIMIT OF USEFUL RESOLUTION DUE TO TRUNCATION OF THE FOURIER SYNTHESIS*

Objective aperture diameter	3.3 mm focal length	1.6 mm focal length
μ	A	A
50	5.5	2.7
30	9.2	4.5
20	13.8	6.7

* The radial position, within the back focal plane, for a given Bragg maximum is calculated from the equation $R = \lambda f/d$; d = the characteristic dimension or lattice periodicity, λ = electron wavelength, and f = objective lens focal length.

the contrast signal, sometimes referred to as "amplitude" contrast, is assumed to be proportional to the amount of scattering which falls beyond the objective aperture opening. If, however, the conditions of plane-wave optics are applicable the analogy with localized absorption in the specimen is not appropriate, since the distribution of the scattering amplitude over the back focal plane is in no way related to absorption processes. The actual contrast that is produced in a Fourier image is a function of not only the magnitudes but also the phases of the various scattering amplitudes. It is difficult, therefore, to make generalized statements as to the effect upon contrast that might be expected at various spatial-frequency truncations (with different-sized apertures). Experimental analysis of contrast effects is complicated by the large proportion of inelastically scattered electrons in the usual (unfiltered) image, and by phase modulation due to lens aberrations. The contrast effects of truncation can be calculated for representative model situations, and such numerical experiments are now in progress. Furthermore it should also be expected that these contrast effects may in the future be important in the quantitative interpretation of filtered images.

Experimental Examples of Low-Angle Fourier Contrast with Biological Specimens

In order to determine whether the approximation of coherent plane-wave scattering (Fraunhofer diffraction) and subsequent Fourier imaging is applicable to electron microscopy of biological specimens it is first necessary to demonstrate the existence of a low-angle diffraction pattern for such specimens. Coherent plane-wave scattering is most easily demonstrated with highly ordered or crystalline structures because of the sharpness of the scattering maxima. The theory applies equally well, however, to structures with no internal periodicity. If a diffraction pattern is observed it is then necessary to confirm that the observed image is consistent, in the nature of its structure, with the observed diffraction pattern. A final test of the hy-

pothesis would be to determine whether the observed image contrast could be quantitatively predicted from the observed scattering amplitude. This final test is not presently possible since it requires image data and diffraction data from which the inelastically scattered electrons have been removed. The measurement of the magnitude of the forward-scattered intensity and the measurement of the complex phases would also present experimental difficulties.

A number of authors have recently obtained low-angle electron diffraction patterns with biological specimens, but these have not been discussed extensively in relation to Fourier imaging. The type of specimen used has included both ordered and random arrays of polystyrene latex spheres (Ferrier and Murray, 1966; Smart and Burge, 1965; Yeh and Geil, 1967), crystalline proteins (Ferrier and Murray, 1966; Murray and Ferrier, 1968), and partially oriented fibers of viruses and collagen (Smart and Burge, 1965; Murray and Ferrier, 1968).

As a first example of a specimen exhibiting a low-angle electron diffraction pattern it is convenient to examine a single-particle layer of "880 A" polystyrene latex spheres. This can be formed by air-drying a dilute suspension of particles on a smooth substrate (e.g. freshly cleaved mica). The particles gather together under the receding meniscus, and the resulting close-packed array can be stripped from the substrate with a carbon replica. The general nature of such a specimen and its resulting diffraction pattern is demonstrated in Fig. 9. The inset at the left center is a very low magnification micrograph of the sheet, showing that the replica is somewhat buckled. The spheres are packed hexagonally in rather small domains but "crystallographic" order appears to extend rather well from one domain to another. The insets at the top show the low-angle diffraction patterns recorded from a selected area of this field with exposure times ranging from ½ to 10 sec. The inset at the top right in Fig. 9 shows an enlargement of one of the hexagonal domains.

A sheet of hexagonally packed spheres can be described mathematically as the convolution of a single sphere with a two-dimensional hexagonal point-lattice. The corresponding Fourier transform is the product of the transform for the lattice and the transform for the sphere. The transform of the lattice is a hexagonal lattice of rods or lines, while the transform of a uniform sphere has spherical symmetry about the origin in reciprocal space, but varies radially according to the Bessel function of 3/2 order (Beeman et al., 1957). The way in which the specimen is oriented relative to the incident beam determines the way in which the Ewald sphere intersects this Fourier transform, and thereby influences the type of diffraction pattern observed.

The type of diffraction pattern produced will influence in turn the type of Fourier contrast image that results. Fig. 10 shows, at a higher magnification, some selected portions from the region of the specimen which is buckled (Fig. 9). As the object plane becomes tilted relative to the incident wave vector the intersection of the Ewald sphere with the Fourier transform can occur at nodes in the transform, or

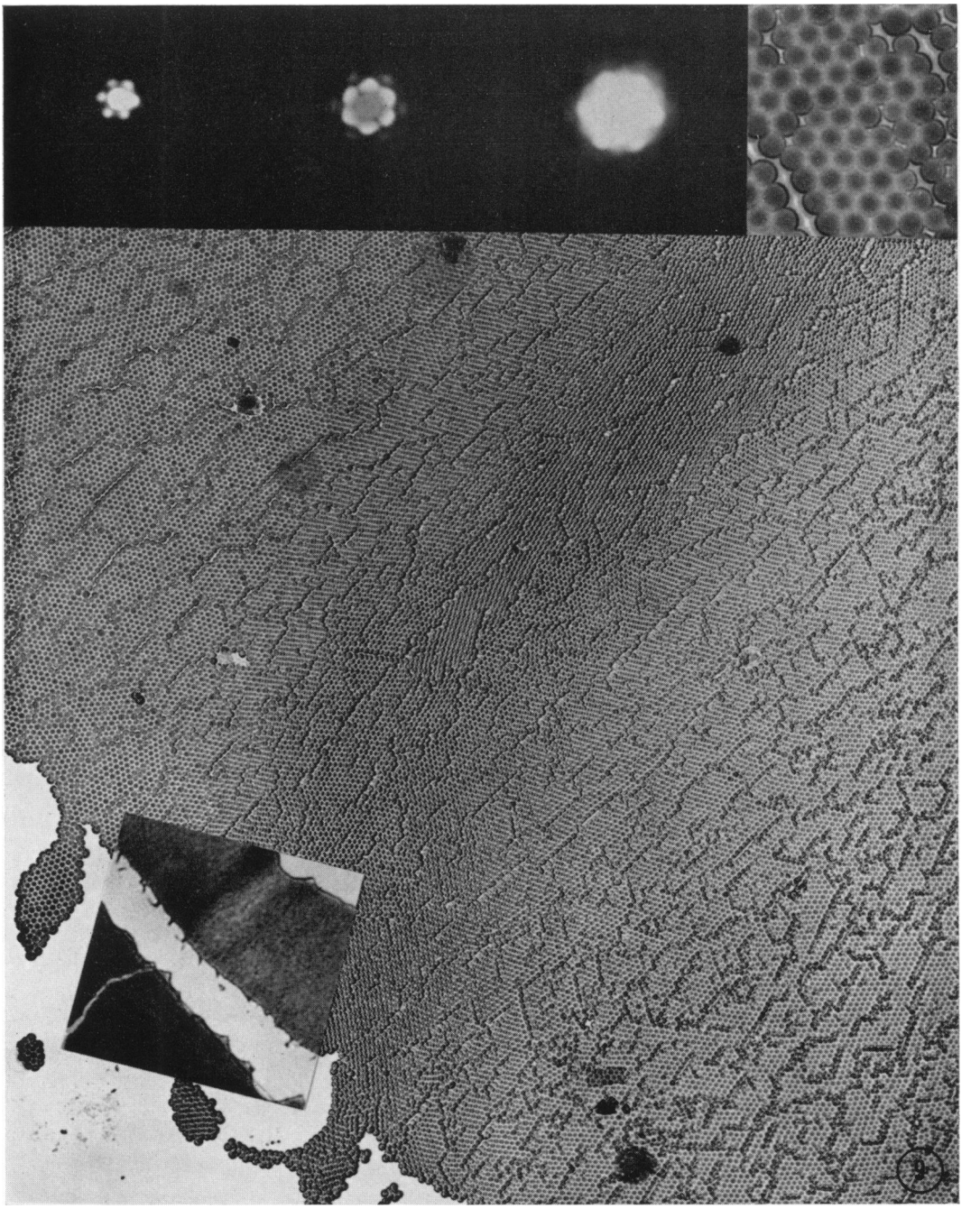

FIGURE 9 Two dimensional sheet of "880 A" diameter polystyrene latex particles in hexagonally packed domains. A region of tilt or warping passes diagonally through the middle of the sheet, and this is shown more clearly in the low magnification inset at the lower left. The inset at top right shows the hexagonal packing of spheres, and the low-angle diffraction patterns obtained with different exposures are also shown as insets at the top of the figure.

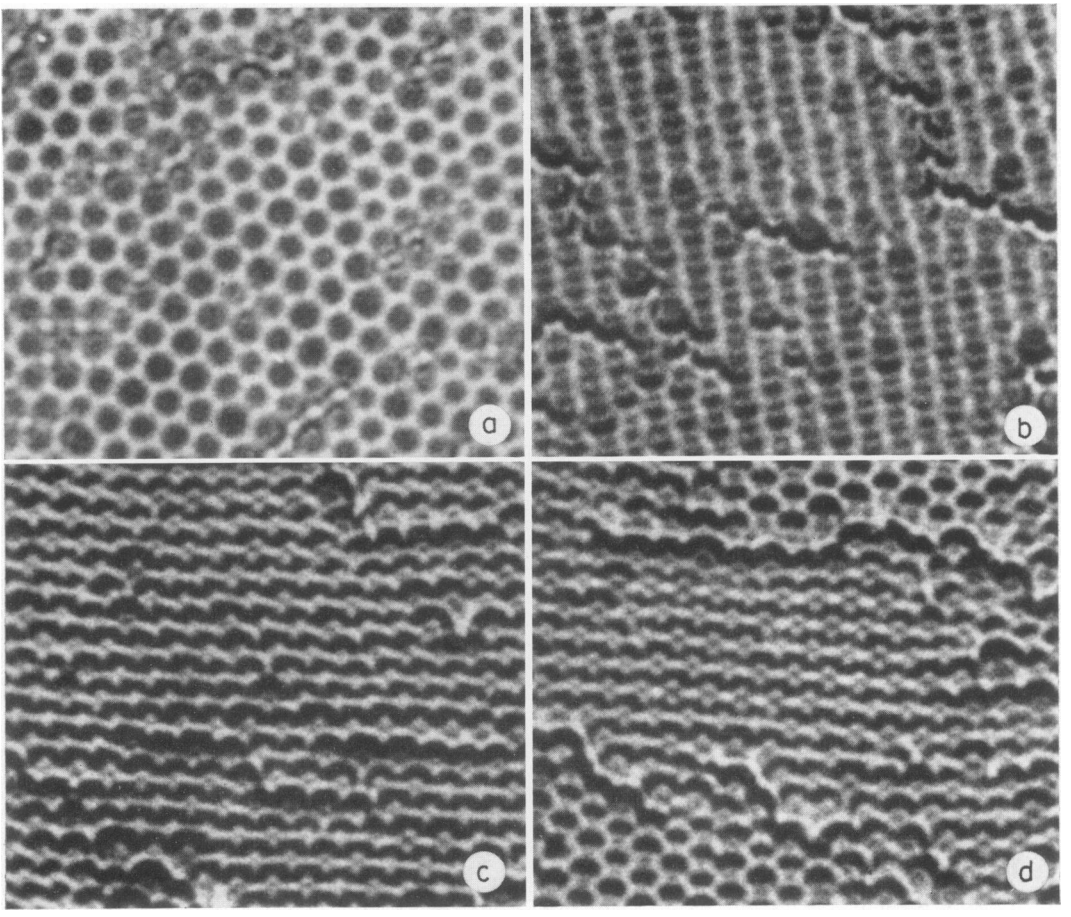

FIGURE 10 Variations in low-angle Fourier contrast as a function of specimen tilt. Selected areas from the same micrograph as shown in Fig. 9 are presented here at higher magnification. In the region of specimen tilt, one can observe a great variety of linear and serrated images which differ remarkably from the image of hexagonally packed spheres obtained when the incident wave vector is normal to the plane of the specimen.

otherwise produce a diffraction pattern that departs remarkably from a hexagonally symmetrical pattern. The type of intersection obtained depends upon the azimuthal rotation of each hexagonal domain as well as the angular tilt, and consequently a variety of linear and serrated images, as in Fig. 10, can occur. We mention especially Figure 10 *d*, in which a nearly hexagonal domain structure is produced at the top right and the bottom left, but evidently a partial rotation of the central domain produces a highly serrated image. Similar variations in the image have been obtained by purposely tilting the specimen stage in order to change the orientation and hence the diffraction pattern. Since the basic subunit of this structure is purely spherical, it is evident that one must be careful in the interpretation of angular or

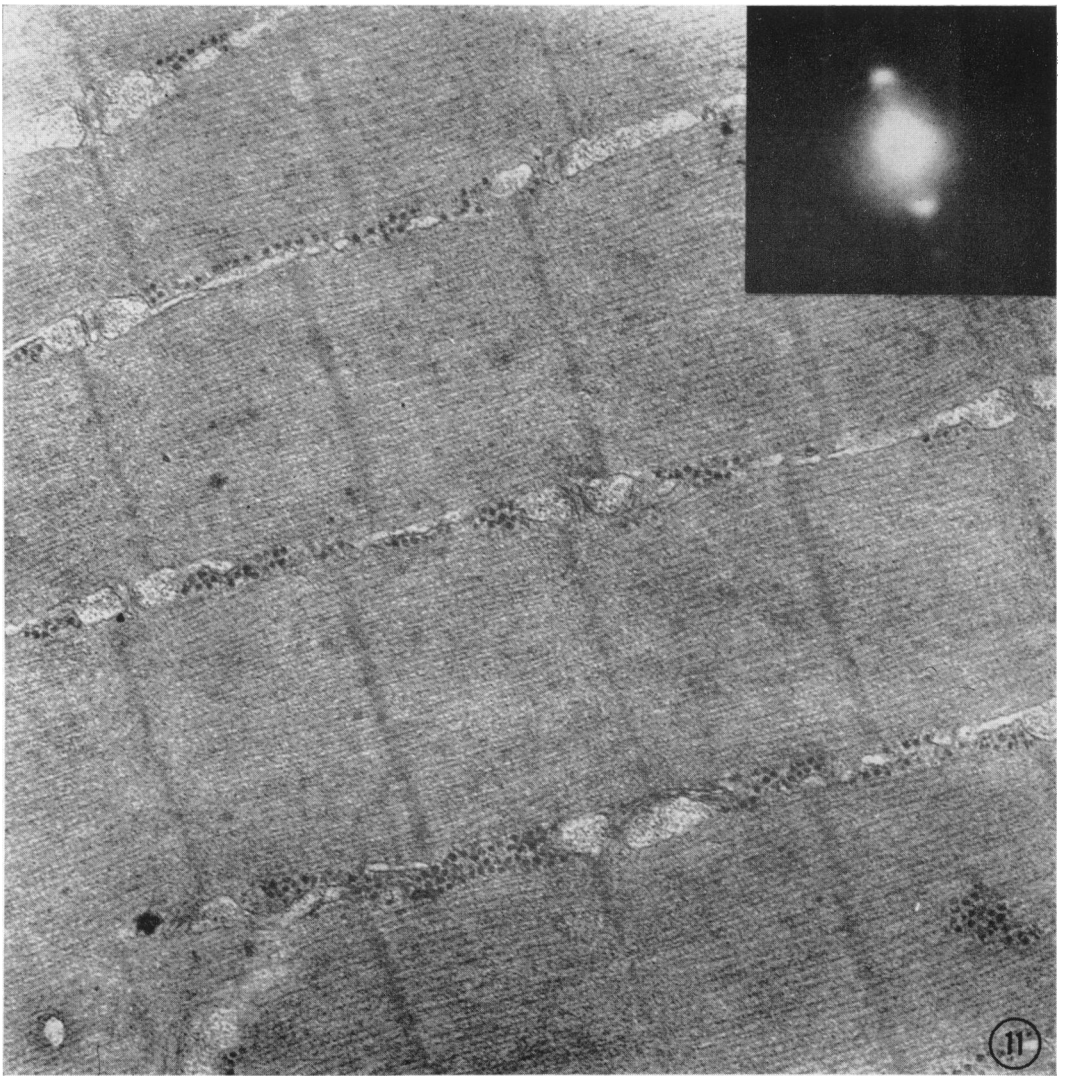

FIGURE 11 Longitudinal thin section of frog skeletal muscle. The muscle was fixed with gluteraldehyde and OsO_4, and sections were stained with uranyl acetate and lead citrate. The inset shows the low-angle electron diffraction pattern obtained from this specimen. The contrast in the diffraction pattern has been manipulated during the photographic transfer in order to better demonstrate the (1, 1) reflection.

serrated image-structures which can result, for example, in Fourier images of protein crystals (Valentine, 1964).

Longitudinal thin sections of striated muscle also provide a convenient specimen for low-angle electron diffraction. Frog skeletal muscle was fixed in situ with phosphate-buffered gluteraldehyde, small pieces of tissue were dissected and post-fixed

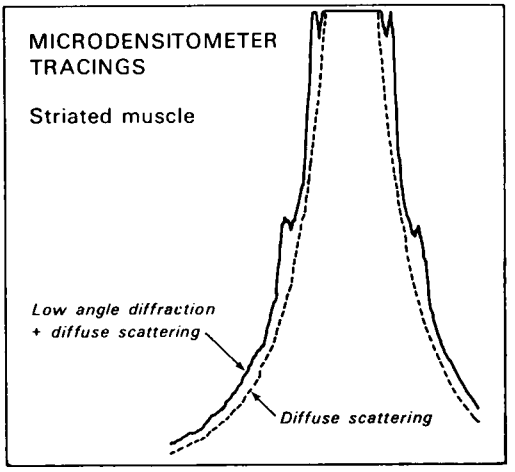

FIGURE 12 Microdensitometer scans recorded from the original low-angle diffraction pattern shown as an inset in Fig. 11. The diffraction pattern was scanned in a line intersecting all four maxima, while the curve labeled "diffuse scattering" was obtained by scanning perpendicular to this.

with phosphate-buffered OsO_4, and the material was embedded in epon in the usual way (Luft, 1961). Thin sections were stained with uranyl acetate and with lead citrate. Fig. 11 shows an electron micrograph of such a longitudinal thin section. The low-angle electron diffraction pattern obtained from an area including that in the micrograph is shown in the inset. Fig. 12 shows microdensitometer tracings that were obtained from the original photographic plate. In this case the effective diffraction-camera length was determined immediately previous to the experiment, using both the image and the low-angle diffraction pattern produced by a polystyrene-sphere specimen. The two equatorial maxima in the diffraction pattern were measured at Bragg spacings of 370 and 215 A. The probable error in these measurements is not more than approximately ± 10 A, part of which is due to a small ambiguity in determining the peak of the diffraction maxima, and part of which is due to instrumental variation of the camera length. The latter can change by as much as 10% unless the lens currents and high voltage are left running continuously between a calibration run and an actual experiment.

The electron diffraction data obtained with the thin sections agree remarkably well with the low-angle X-ray scattering data reported in the literature for frog skeletal muscle. Huxley first reported a Bragg spacing of 380 $\pm$ 15 A for the 1, 0 equatorial reflection with living frog sartorius muscle (Huxley, 1953), while Elliot et al. have reported a spacing of 343 $\pm$ 12 A with similar preparations (Elliot, Lowy, and Worthington, 1963). It has recently been shown that the fundamental lattice dimension in frog muscle can vary from about 400 A to about 460 A depending upon sarcomere length and upon the live versus the rigor state of the muscle. The X-ray data have been interpreted as representing the scattering from a hexagonal lattice of myosin filaments, which are in turn surrounded by actin filaments in the region of the sarcomere where the two interdigitate (Huxley and Hanson, 1960; Elliot, Lowy, and Worthington, 1963).

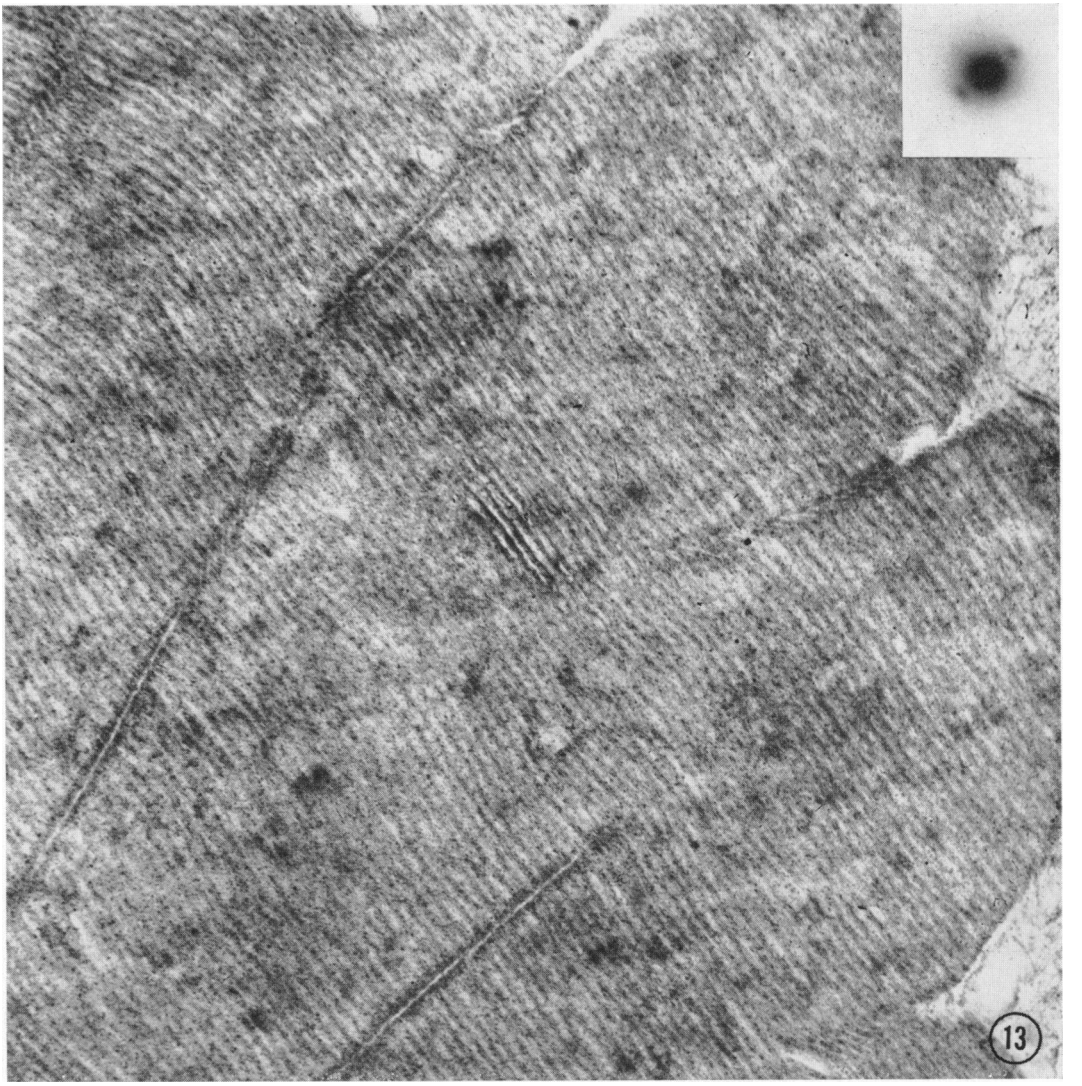

FIGURE 13 Thin section through the layered membrane structure of the frog retinal rod. The tissue was fixed with gluteraldehyde and OsO_4, and sections were stained with uranyl acetate and lead citrate. The membranes are approximately parallel to each other with a center to center spacing of about 300 A, but some bending and warping does occur. The inset shows the low-angle electron diffraction pattern obtained from the same structure. The diffuse maxima at approximately 300 A are consistent with the ordered but not crystalline structure seen in the micrograph.

From the electron diffraction data reported here one would estimate that the center-to-center spacing of the myosin filaments in these specimens was 430 A. However, the only *periodic* structure seen in the micrographs is that of the 370 and 215 A lattice planes. For longitudinal sections the only circumstances under which

the 430 A spacing could be observed in the diffraction pattern and in the image would be if the specimen was perfectly oriented along a row of filaments and if the section was only one filament thick.

As a third example of low-angle Fourier contrast it is possible to record the diffuse maxima in the low-angle scattering pattern from the ordered, but certainly not crystalline, membranes of the visual receptor structure in frog retina. Specimens were prepared by the same technique described above for skeletal muscle. Fig. 13 is a micrograph of a single rod outer segment, for which the plane of the layered membranes was approximately perpendicular to the plane of the section. The inset shows the low-angle diffraction pattern obtained from the same layered-membrane structure. The diffuseness of the maxima is not surprising in view of the variation in distances between individual membranes and the variation in the degree of membrane-tilt within the section.

The work reported here was conducted in part through the support of the A.E.C. and the U.S.P.H.S.

We wish also to acknowledge the assistance of several individuals who have contributed to the preparation of specimens and the analysis of data: Dr. L. R. Adams, Dr. W. G. Brammer, Miss Jessie Hsu, Miss Jerri Hirschberg, Miss Sue Daniels, Mr. Paul Aebersold, and Mrs. Thea Scott.

Received for publication 7 February 1969.

REFERENCES

ABBE, E. 1873. *Archiv Mikroskopische Anatomie.* **9**:413.

ANDERSON, T. F. 1956. *Proc. Intern. Conf. Electron Microscopy, 3rd, London, 1954.* pp. 122–128.

BASSETT, G. A., and A. KELLER. 1964. *Phil. Mag.* **9**:817.

BEEMAN, W. W., P. KAESBERG, J. W. ANDEREGG, and M. B. WEBB. 1957. Handbuch d. Physik. Springer Verlag, Berlin. **32**:321.

COWLEY, J. M., and A. F. MOODIE. 1957 a. *Proc. Phys. Soc. (London)* **B70**:486.

COWLEY, J. M., and A. F. MOODIE. 1957 b. *Proc. Phys. Soc. (London)* **B70**:497.

COWLEY, J. M., and A. F. MOODIE. 1957 c. *Proc. Phys. Soc. (London)* **B70**:505.

CURTIS, G. H., R. P. FERRIER, and R. T. MURRAY. 1967. *J. Sci. Instrum.* **44**:867.

DEROSIER, D. J., and A. KLUG. 1968. *Nature.* **217**:130.

ELLIOT, G. F., J. LOWY, and C. R. WORTHINGTON. 1963. *J. Mol. Biol.* **6**:295.

FARRANT, J. L. and A. J. HODGE. 1956. *Proc. Intern. Conf. Electron Microscopy, 3rd, London, 1954.*

FERRIER, R. P., and R. T. MURRAY. 1966. *J. Roy. Microsc. Soc.* **85**:323.

FISCHBACH, F. A., and J. W. ANDEREGG. 1965. *J. Mol. Biol.* **14**:458.

GLAESER, R. M., T. HAYES, H. MEL, and C. TOBIAS. 1966. *Exp. Cell Res.* **42**:467.

GLAESER, R. M., and G. THOMAS. Spring, 1968. Semiannual Report Biology and Medicine. Donner Laboratory, University of California, Berkeley. **UCRL-18347**:175.

GLAESER, R. M., G. THOMAS, R. CHRISTENSEN, and W. G. BRAMMER. 1968. Proceedings 26th Annual Meeting Electron Microscopy Society America, New Orleans. Claitor Press, New Orleans.

GLAUERT, A. M. 1965. *In* Techniques for Electron Microscopy. D. H. Kay, editor. F. A. Davis, Philadelphia. 2nd edition.

GOODMAN, J. W. 1968. Introduction to Fourier Optics. McGraw-Hill, New York.

GRANICK, S. 1942. *J. Biol. Chem.* **146**:451.

HAAS, D. J. 1968. *Biophys. J.* **8**:549.

HALL, C. E. 1966. Introduction to Electron Microscopy. McGraw-Hill, New York. 2nd edition.

HEIDENREICH, R. D. 1964. Fundamentals of Transmission Electron Microscopy. Interscience, New York.

HIRSCH, P. B., A. HOWIE, R. B. NICHOLSON, D. W. PASHLEY, and M. J. WHELAN. 1965. Electron Microscopy of Thin Crystals. Plenum Press, New York.
HUXLEY, H. E. 1953. *Proc. Roy. Soc. Ser. B Biol. Sci.* **141**:59.
HUXLEY, H. E. 1968. *J. Mol. Biol.* **37**:507.
HUXLEY, H. E. and J. HANSON. 1960. *In* Structure and Function of Muscle. G. Bourne, editor. Academic Press, Inc., New York. **1**.
KOMODA, T. 1966. *In* Electron Microscopy. 1966. R. Uyeda, editor. Maruzen Company, Tokyo. **1**:29.
LENARD, J., and S. J. SINGER. 1968. *J. Cell Biol.* **37**:117.
LUFT, J. H. 1961. *J. Biol. Biochem. Cytol.* **9**:409.
MAHER, D. M., W. L. BELL, and G. THOMAS. 1965. Argonne Conference—Lattice Defects in Quenched Metals. R. M. J. Cotterill, editor. Academic Press, Inc., New York.
MURRAY, R. T., and R. P. FERRIER. 1968. *J. Ultrastruct. Res.* **21**:361.
PARSONS, D. F. 1966. Electron Microscopy. 1966. R. Uyeda, editor. Maruzen Company, Tokyo. **2**:121.
PARSONS, D. F. 1968. *In* International Review of Experimental Pathology. G. W. Richter and M. A. Epstein, editors. Academic Press, New York. **6**.
PEASE, D. C. 1966. *J. Ultrastr. Res.* **14**:356.
PEASE, D. C. 1967. *J. Ultrastr. Res.* **21**:75.
PORTER, A. B. 1906. *Phil. Mag.* **11**:154.
SAGE, H. J., and S. J. SINGER. 1962. *Biochemistry.* **1**:305.
SINGER, S. J. 1962. *Advan. Protein Chem.* **17**:1.
SMART, J., and R. E. BURGE. 1965. *Nature.* **205**:1297.
TANFORD, C., C. E. BUCKLEY III, P. K. DE, and E. P. LIVELY. 1962. *J. Biol. Chem.* **237**:1168.
THOMAS, G. 1962. Transmission Electron Microscopy of Metals. J. Wiley, New York.
TSUBOI, M., T. TAKENISHI, and Y. ITAKA. 1959. *Bull. Chem. Soc. Jap.* **32**:305.
UYEDA, R. 1955. *J. Phys. Soc. Jap.* **10**:256.
UYEDA, R. 1956. *Proc. Intern. Conf. Electron Microscopy, 3rd, London, 1954.*
VAINSHTEIN, B. K. 1964. Structure Analysis by Electron Diffraction. The Macmillan Company, New York.
VALENTINE, R. C. 1964. *Nature.* **204**:1262.
YEH, G. S. Y., and P. H. GEIL. 1967. *J. Mater. Sci.* **2**:457.